Distributed Adaptive Droop Control for DC Distribution Systems

Nasirian, Vahidreza ; Davoudi, Ali; Lewis, Frank; Guerrero, Josep M.

Published in:
I E E E Transactions on Energy Conversion

DOI (link to publication from Publisher):
10.1109/TEC.2014.2350458

Publication date:
2014

Document Version
Publisher's PDF, also known as Version of record

Citation for published version (APA):
Nasirian, V., Davoudi, A., Lewis, F., & Guerrero, J. M. (2014). Distributed Adaptive Droop Control for DC Distribution Systems. *I E E E Transactions on Energy Conversion*, *29*(4), 944-956.
https://doi.org/10.1109/TEC.2014.2350458

Distributed Adaptive Droop Control for DC Distribution Systems

Vahidreza Nasirian, *Student Member, IEEE*, Ali Davoudi, *Member, IEEE*, Frank L. Lewis, *Fellow, IEEE*, and Josep M. Guerrero, *Senior Member, IEEE*

***Abstract*— A distributed-adaptive droop mechanism is proposed for secondary/primary control of dc Microgrids. The conventional secondary control, that adjusts the voltage set point for the local droop mechanism, is replaced by a voltage regulator. A current regulator is also added to fine-tune the droop coefficient for different loading conditions. The voltage regulator uses an observer that processes neighbors' data to estimate the average voltage across the Microgrid. This estimation is further used to generate a voltage correction term to adjust the local voltage set point. The current regulator compares the local per-unit current of each converter with the neighbors' on a communication graph and, accordingly, provides an impedance correction term. This term is then used to update the droop coefficient and synchronize per-unit currents or, equivalently, provide proportional load sharing. The proposed controller precisely accounts for the transmission/distribution line impedances. The controller on each converter exchanges data with only its neighbor converters on a sparse communication graph spanned across the Microgrid. Global dynamic model of the Microgrid is derived, with the proposed controller engaged. A low-voltage dc Microgrid prototype is used to verify the controller performance, link-failure resiliency, and the plug-and-play capability.**

***Index Terms*— Cooperative control, dc-dc converter, dc Microgrid, distributed control, droop control.**

I. INTRODUCTION

Microgrids, as small-scale power systems, are becoming popular in distribution systems [1]–[3]. The dc nature of renewable energy sources, storage elements, or emerging electronics loads favor a dc Microgrid paradigm to avoid redundant dc-ac-dc conversions [4], [5]. Moreover, dc Microgrids can overcome some disadvantages of ac systems, e.g., transformer inrush current, frequency synchronization, reactive power flow, and power quality issues [6]. Resembling the control hierarchy of the legacy grid, a hierarchical control structure is conventionally adopted for Microgrid operation [7]–[10]. The highest level in the hierarchy (tertiary) is in charge of economical dispatch and coordination with the distribution system operator. It assigns the Microgrid voltage to carry out a prescheduled power exchange between the Microgrid and the main grid [11]–[13]. To satisfy the voltage demand of the tertiary control, the secondary control measures voltages across the Microgrid and, accordingly, updates the voltage set points for the primary controllers. The primary control, typically implemented locally on individual converters with a droop mechanism, regulates the output voltage of individual converters and handles load sharing among sources.

The secondary and tertiary controls are typically implemented in a centralized fashion [14], where a central entity communicates with converters through a highly-connected communication network. Loss of any link in such topologies can lead to the failure of the corresponding unit, overstressing other units, and potentially leading to system-level instability and cascaded failures [15]. Since future extensions add to the controller complexity, scalability is not straightforward. Distributed control has emerged as an attractive alternative as it offers improved reliability, simpler communication network, and easier scalability [16]. For example, distributed tertiary control via dc bus signaling is studied in [17], [18]. Structurally, it is desirable to extend the distributed control paradigm to the secondary/primary levels. Categorically, such a controller shall satisfy two main control objectives of dc Microgrids, namely voltage regulation [19] and proportional load sharing [20].

Proper load sharing assigns the load among participating converters in proportion to their rated powers (or, equivalently, rated currents). This approach equalizes the per-unit currents of all sources, and prevents circulating currents [20] and overstressing of any source [21]. The droop control is widely adopted for load sharing by imposing virtual output impedance on each converter [22], [23]. Static/dynamic performance and stability assessment of droop controllers are investigated in [1], [24], and [25]. Constant droop is commonly used for power reference tracking and load sharing in grid-connected and islanded modes, respectively [26], [27]. However, its load sharing performance is susceptible to transmission line impedances [28]. Generally, higher droop coefficients result in improved load sharing, however, at the cost of further degrading the voltage regulation. Thus, to achieve a desirable load sharing, the droop coefficients should vary to account for line impedances and load variations.

Manuscript received May 02, 2014; accepted August 11, 2014. Part of the work was presented at the 2014 IEEE Applied Power Electronics Conference and Exposition, Fort Worth, TX, USA, March 16–20. This work was supported in part by the National Science Foundation under grants ECCS-1137354 and ECCS-1128050 and in part by the U.S. Office of Naval Research under grant N00014-14-1-0718.

Authors are with the University of Texas at Arlington Research Institute, Fort Worth, TX 76118 USA (emails: vahidreza.nasirian@mavs.uta.edu; davoudi@uta.edu; lewis@uta.edu). Josep M. Guerrero is with the Department of Energy Technology, Alborg University, Denmark (joz@et.aau.dk).

Moreover, since some sources (e.g., PV-driven modules or storage devices) lack a constant rated power, dynamic adjustment of droop coefficients is required as their rated power changes [29].

A piece-wise linear droop mechanism in [28] and [30] uses two different droop gains for low and high powers. The idea is further developed in [31] and [32] where droop coefficients continuously vary in response to change in power. This approach improves voltage regulation; however, voltage drop across the Microgrid is still noticeable. This method is developed for two-agent systems and extension to a multi-converter system is not straightforward. Moreover, improved voltage regulation has compromised accurate proportional load sharing. Adaptive-droop control for power flow control in grid-connected mode is studied in [33], [34]. Droop gains are adjusted in reciprocal to power demand in [35] where communication of a synchronization signal is needed among all converters. This requirement, in turn, compromises the plug-and-play capability. Decentralized [21] and supervisory [36] adaptive-droop approaches formulate droop gains in terms of batteries' state of charges [37].

Existing droop mechanisms generally suffer from poor voltage regulation and load sharing, particularly when the distribution line impedances are not negligible [38]–[40]. Possible solutions to the aforementioned issues have been reviewed in [16]. These solutions are either structured centrally [7] or require development of a fully connected data exchange network across the Microgrid, where any two nodes are in direct contact [22], [41]–[43]. Assuming equal voltages for all converters across the Microgrid in [7] is not practical, particularly, in dc distribution systems. Point-to-point communication links are required for all sources in [44], where any link failure renders the whole Microgrid inoperable. The line impedance is taken into account in [45], where the data exchange requires a fully connected communication graph. Proper operation of the controller demands information of all nodes and, thus, any link failure impairs the whole control functionality. Scalability is another challenge; after any structural/electrical upgrade, some control settings, e.g., the number of sources, need to be updated and embedded in all converters.

The voltage regulation requirement is redefined in [46] to incorporate the line impedance effect. The average voltage across the Microgrid (and only not a specific bus voltage) should be regulated at the global voltage set point determined by the tertiary control. This is called the *global voltage regulation*, and is considered here. Tertiary control levels would involve distributed optimization techniques to implement economical dispatch and/or loss optimization, and is the subject of future work. This paper focuses on the secondary/primary control of the dc Microgrids and offers the following contributions:

- Each converter is augmented with a current regulator that compares the actual per-unit current of that converter with a weighted average of its neighbors' and, accordingly, generates an impedance correction term to adjust droop coefficient and, thus, provide proportional load sharing.
- A voltage regulator is also added. This regulator uses the estimation made by a voltage observer to adjust the local voltage set point and provide global voltage regulation.
- The voltage observer processes neighbors' data and local voltage measurement through a so-called *dynamic consensus* protocol to estimate the global average voltage.
- Cooperation of the voltage and current regulators is shown to effectively carry out both global voltage regulation and proportional load sharing, particularly, when the line impedances are not negligible.
- A sparse communication network is spanned across the Microgrid to enable limited message passing among converters; each converter only exchanges data with its neighbors. This is in direct contrast to the centralized control approaches that require communication networks with high-bandwidth communication links and a high level of connectivity.
- This adaptive droop approach expands the work of authors in [46] and achieves a faster load sharing dynamics.
- Compared to the existing techniques (e.g., [45]) the control scheme employs a truly distributed approach that does not require a priori knowledge of the global parameters such as the number of sources. Thus, it is scalable and suitable for the plug-and-play operation.
- Unlike existing methods that require fully connected graphs and may fail in case of any communication link failure, the proposed method is not susceptible to any single link failure, which leads to a more reliable control framework.

The rest of this paper is outlined as follows: Section II introduces the distributed control paradigm. The cooperative adaptive-droop control is discussed in Section III. Section IV, explains functionality of the voltage observer. Global dynamic and static models are studied in Section V. The controller performance is verified using a low-voltage dc Microgrid prototype in Section VI. Section VII concludes the paper.

II. Distributed Cooperative Control Framework

Microgrid sources are mapped to a cyber network as shown in Fig. 1, where each node represents an active source (or, converter) and each edge represents a communication link for data exchange. The communication graph might have a different topology than the underlying physical Microgrid. This cyber connection sets the groundwork for the cooperative control paradigm, where neighbors' interactions can lead to a global consensus. Accordingly, not all agents (converters) in a large-scale dynamic system need to be in direct contact. Instead, each agent only communicates its control variables with its neighbors. Then, using the neighbors' data and its local measurements, the agent updates its control variables. The cooperative control offers global consensus of the desired variables, shall the communication graph be designed properly.

A directed graph (digraph), associated with the cyber layer in Microgrid, is highlighted in Fig. 1.

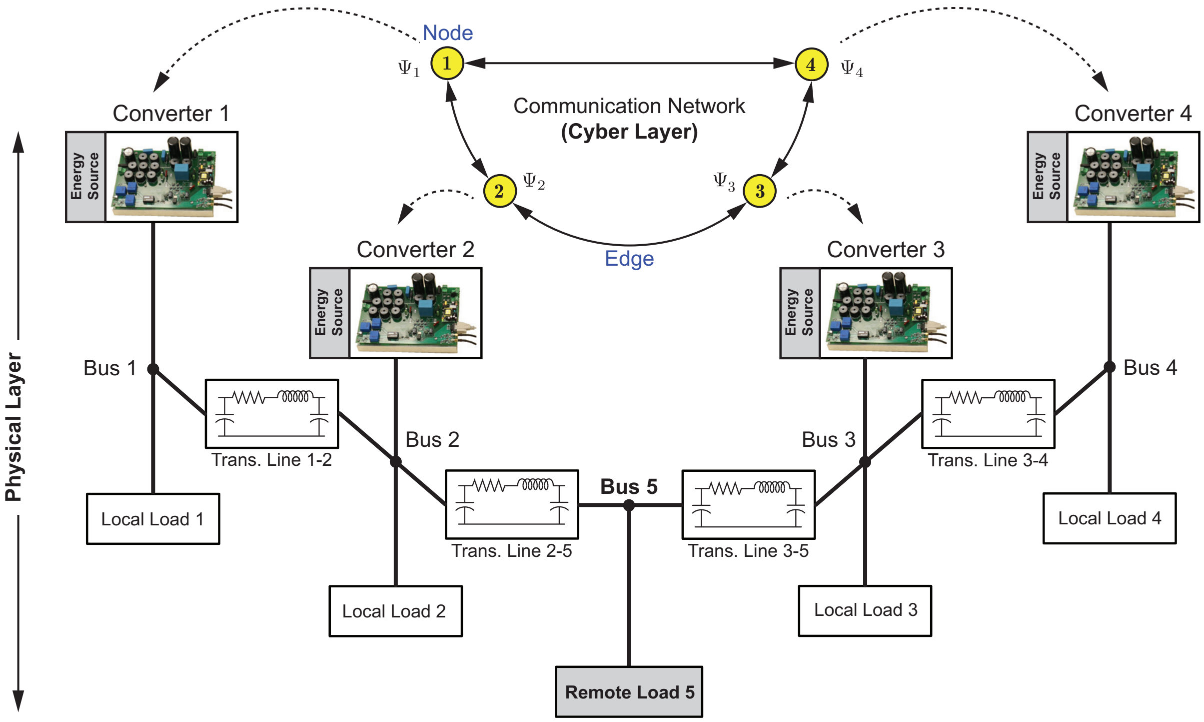

Fig. 1. General layout of a dc Microgrid including energy sources supplying the grid and the cyber network facilitating data exchange among sources.

Such a graph is usually represented as a set of nodes $\mathbf{V_G} = \{v_1^g, v_2^g, ..., v_N^g\}$ connected via a set of edges $\mathbf{E_G} \subset \mathbf{V_G} \times \mathbf{V_G}$, and an associated adjacency matrix $\mathbf{A_G} = [a_{ij}] \in \mathbb{R}^{N\times N}$. The Adjacency matrix $\mathbf{A_G}$ contains communication weights, where $a_{ij} > 0$ if $(v_j^g, v_i^g) \in \mathbf{E_G}$ and $a_{ij} = 0$, otherwise. a_{ij} is the communication weight for data transfer from node j to node i. Here, a time-invariant adjacency matrix is assumed. $N_i = \{j \mid (v_j^g, v_i^g) \in \mathbf{E_G}\}$ denotes the set of all neighbors of node i, i.e., if $j \in N_i$, then v_i^g receives information from v_j^g. However, in a digraph, the link is not necessarily reciprocal, i.e., v_j^g might not receive information from v_i^g. The in-degree matrix $\mathbf{D_G^{in}} = \mathrm{diag}\{d_i^{in}\}$ is a diagonal matrix with $d_i^{in} = \sum_{j\in N_i} a_{ij}$. Similarly, the out-degree matrix is $\mathbf{D_G^{out}} = \mathrm{diag}\{d_i^{out}\}$, where $d_i^{out} = \sum_{i\in N_j} a_{ji}$. The Laplacian matrix is then defined as $\mathbf{L} = \mathbf{D_G^{in}} - \mathbf{A_G}$, whose eigenvalues determine the global dynamics [47]. The Laplacian matrix is balanced if the in-degree of each node matches its out-degree, i.e., $\mathbf{D_G^{in}} = \mathbf{D_G^{out}}$. Particularly, if the graph is undirected, i.e., all links are bidirectional, then the Laplacian matrix is balanced. A direct path from v_i^g to v_k^g is a sequence of edges that connects the two nodes. A digraph is said to have a spanning tree if it contains a root node, from which there exists at least a direct path to every other node.

The physical layer of the Microgrid, shown in Fig. 1, includes dispatchable sources (including the power converters), transmission lines, and loads. The cyber layer, comprised of all communication links, is spanned among the sources to facilitate data exchange. This is a sparse communication network with at least one spanning tree. In addition, the graph is chosen such that in case of any link failure the remaining network still contains at least one spanning tree. This redundancy is required to ensure link-failure resiliency. Each converter broadcasts a data set, Ψ_i, to its neighbors. The data package transmitted by node i, $\Psi_i = [\overline{v}_i, i_i^{pu}]$, consists of two elements; its estimate of the average voltage across the Microgrid, $\overline{v}_i$, and the measured per-unit current, i_i^{pu}. The term per-unit here refers to the current provided by the converter divided by its rated current, i.e., $i_i^{pu} \triangleq i_i / I_i^{rated}$, where i_i and I_i^{rated} are the supplied and rated currents of the i–th converter, respectively. This terminology of the per-unit is used here to represent loading percentage of each converter. At the receiving ends of the communication links, each converter k receives data from all its neighbors, Ψ_j, $j \in N_k$, with associated communication weights, a_{kj}. These weights are design parameters and can be considered as data transfer gains.

III. Adaptive Droop Control

The global voltage regulation and proportional load sharing are the two objectives of the secondary control, which require proper voltage set point assignment for individual converters. The proposed secondary controller is elaborated in Fig. 2(a), where local and neighbors' information are processed to adjust the local voltage set point, v_i^*. Cooperation among converters, at the secondary control level, helps to fine-tune the voltage set points, v_i^*, and mitigate the current and voltage residues.

The voltage set point for each converter is augmented with two terms provided through cooperation among converters. They are resulted from voltage and current regulators. Based on Fig. 2(a), the local voltage set point for an individual converter can be expressed as

$$v_i^* = v_i^{ref} - v_i^d + \delta v_i = v_i^{ref} - r_i i_i + \delta v_i, \tag{1}$$

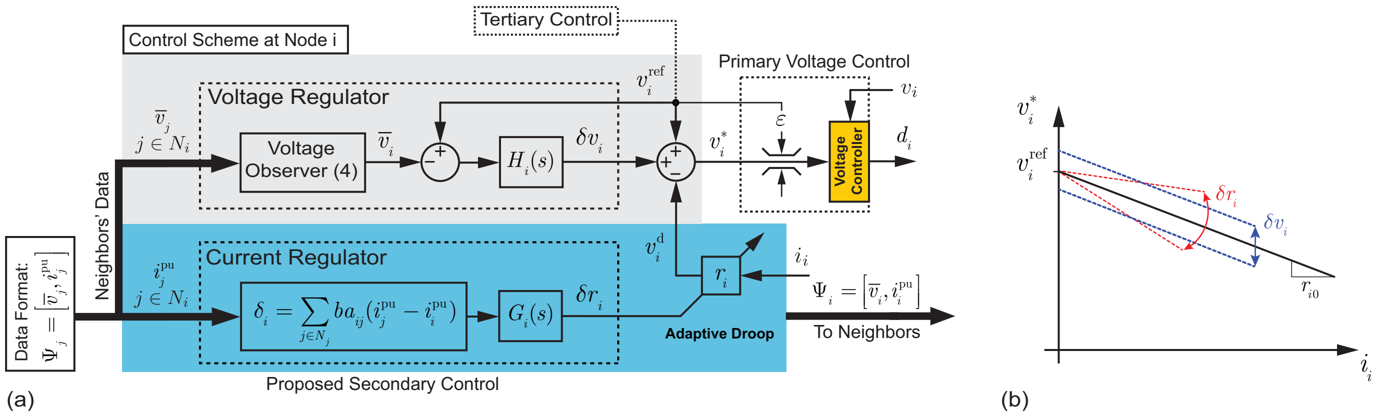

Fig. 2. Proposed distributed control policy: (a) cooperative adaptive droop control for a single agent (converter), (b) effect of adjustable voltage correction and virtual impedance on the droop characterization.

where v_i^{ref}, v_i^{d}, δv_i, and r_i are the global reference voltage, droop voltage, voltage correction term, and the virtual impedance of the i–th converter, respectively. This set point is further adjusted by a voltage limiter (see Fig. 2(a)) to maintain the bus voltages within an acceptable range. Figure 2(b) elaborates how adjustable voltage correction term, δv_i, and virtual impedance, r_i, can navigate operating point of the converter. The droop mechanism, which generates the term $r_i i_i$ in (1), characterizes output impedance of the converters and helps to share load, which leads to the voltage drop across the Microgrid. The voltage correction terms, δv_i s, are augmented to the local reference voltages to boost the voltage across the Microgrid. Accordingly, the controller contains two modules; a voltage regulator and a current regulator.

The voltage regulator at node i consists of a voltage observer and a PI controller, $H_i(s)$. The voltage observer at each node estimates the averaged voltage across the Microgrid, where $\overline{v}_i$ is the estimation at node i. This estimation is then compared with the global reference voltage, v_i^{ref}, to generate the voltage correction term, δv_i. In case of any mismatch between $\overline{v}_i$ and v_i^{ref}, the controller adjusts δv_i to eliminate the discrepancy. In the islanded mode of operation, the global reference voltages, v_i^{ref} s, are typically identical and equal to the rated voltage of the Microgrid. However, in the grid-tied mode, the tertiary control sets a new voltage level for the Microgrid and relays the new reference values to individual converters. A cooperative observer will process the local voltage measurement and the neighbors' estimates to evaluate the average voltage across the Microgrid. Functionality of the observer is discussed in detail in Section IV.

The current regulator at node i provides the input to the droop mechanism. The droop mechanism characterizes the converter output impedance using the virtual impedance r_i. Virtual impedances are conventionally initialized in reciprocal to the converters' rated current, i.e., $r_{i0} = m/I_i^{\mathrm{rated}}$, where m is a design parameter and is identical for all converters. However, the distribution line impedances compromise performance of the droop controller. Thus, the droop gains are suggested to adapt according to the Microgrid loading condition. To this end, a cooperative current regulator is included in the secondary control of any converter, e.g., converter i, which compares local per-unit current, i_i^{pu}, with the weighted average of the neighbors' per-unit currents and finds the current mismatch, δ_i,

$$\delta_i = \sum_{j \in N_i} b a_{ij} (i_j^{\mathrm{pu}} - i_i^{\mathrm{pu}}). \tag{2}$$

where b is the coupling gain between the voltage and current regulators. This mismatch is then fed to a PI controller, $G_i(s)$, to generate an impedance correction term, δr_i, which updates the virtual impedance,

$$r_i(t) = r_{i0} - \delta r_i(t). \tag{3}$$

If the per-unit currents of any two neighbors' differ, the current regulators of the corresponding converters respond and adjust their impedance correction terms to achieve balance.

IV. Voltage Observer

The observer is the primary stage of the voltage regulator module, as shown in Fig. 2. It uses a dynamic cooperative framework to process local and neighbors' information and estimate the average voltage across the Microgrid. Figure 3 explains the distributed cooperative policy for global averaging. The observer at node i receives its neighbors' estimates, $\overline{v}_j$ s ($j \in N_i$). Then, the observer updates its own estimate, $\overline{v}_i$, by processing the neighbors' estimates and the local voltage measurement, v_i,

$$\overline{v}_i(t) = v_i(t) + \int_0^t \sum_{j \in N_i} a_{ij} \left(\overline{v}_j(\tau) - \overline{v}_i(\tau) \right) \mathrm{d}\tau. \tag{4}$$

This updating protocol is referred to as *dynamic consensus* in the literature [48]. As seen in (4), the local measurement, i.e., v_i, is directly fed into the estimating protocol. Thus, in case of any voltage variation at node i, the local estimate, $\overline{v}_i$, immediately responds. Then, the change in $\overline{v}_i$ propagates through the communication network and affects all other estimations.

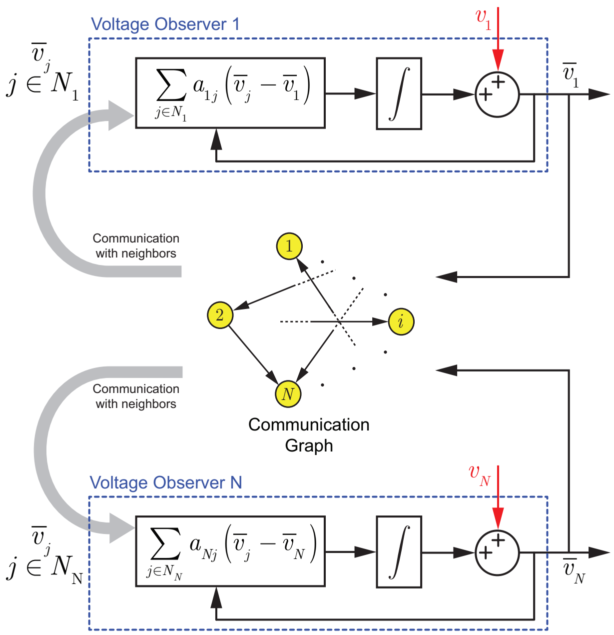

Fig. 3. Dynamic consensus protocol for averaging voltage across a Microgrid; estimating policy at each node.

By differentiating (4),

$$\dot{\overline{v}}_i = \dot{v}_i + \sum_{j\in N_i} a_{ij}\left(\overline{v}_j - \overline{v}_i\right) = \dot{v}_i + \sum_{j\in N_i} a_{ij}\overline{v}_j - d_i^{\mathrm{in}}\overline{v}_i. \tag{5}$$

The global observer dynamic can be formulate accordingly,

$$\dot{\overline{\mathbf{v}}} = \dot{\mathbf{v}} - \left(\mathbf{D}_{\mathbf{G}}^{\mathrm{in}} - \mathbf{A}_{\mathbf{G}}\right)\overline{\mathbf{v}} = \dot{\mathbf{v}} - \mathbf{L}\overline{\mathbf{v}}, \tag{6}$$

where the voltage measurement vector, $\mathbf{v} = [v_1, v_2, \ldots, v_N]^{\mathrm{T}}$, carries measured voltage of all nodes. Similarly, the voltage estimation vector, $\overline{\mathbf{v}} = [\overline{v}_1, \overline{v}_2, \ldots, \overline{v}_N]^{\mathrm{T}}$, contains the global average voltage estimated by all nodes. Equivalently, in the frequency domain,

$$s\overline{\mathbf{V}} - \overline{\mathbf{v}}(0) = s\mathbf{V} - \mathbf{v}(0) - \mathbf{L}\overline{\mathbf{V}}, \tag{7}$$

where $\mathbf{V}$ and $\overline{\mathbf{V}}$ are the Laplace transforms of $\mathbf{v}$ and $\overline{\mathbf{v}}$, respectively. Equation (4) implies that $\mathbf{v}(0) = \overline{\mathbf{v}}(0)$. Therefore,

$$\overline{\mathbf{V}} = s(s\mathbf{I}_N + \mathbf{L})^{-1}\mathbf{V} = \mathbf{H}_{\mathrm{obs}}\mathbf{V}, \tag{8}$$

where $\mathbf{I}_N \in \mathbb{R}^{N\times N}$ and $\mathbf{H}_{\mathrm{obs}}$ are the identity matrix and the observer transfer function, respectively. Equation (8) represents the global dynamics of the voltage observers. It is shown in [46] that if $\mathbf{L}$ is balanced, then all entries of the voltage estimation vector, $\overline{\mathbf{v}}$, converge to a consensus value, which is the true average voltage, i.e., the average of all entries in $\mathbf{v}$. In other words,

$$\overline{\mathbf{v}}^{\mathrm{ss}} = \mathbf{Q}\mathbf{v}^{\mathrm{ss}} = \left\langle \mathbf{v}^{\mathrm{ss}} \right\rangle \underline{\mathbf{1}}, \tag{9}$$

where $\mathbf{Q} \in \mathbb{R}^{N\times N}$ is the averaging matrix, whose elements are all equal to $1/N$. $\underline{\mathbf{1}} \in \mathbb{R}^{N\times 1}$ is a vector whose elements are all equal to one. $\mathbf{x}^{\mathrm{ss}}$ and $\langle \mathbf{x} \rangle$ represent the steady-state value of the vector $\mathbf{x} \in \mathbb{R}^{N\times 1}$ and the average of all vector elements, respectively.

V. Global Model Development

Global model development is essential to study how the proposed controller affects the transient response and steady-state operation of the Microgrid. This model can be used to tune the design parameters and achieve any desired dynamic.

A. Global Dynamic Model

Switching nature of power electronic converters can potentially result in a nonlinear system. Accordingly, small-signal methods are commonplace for dynamic characterization purposes (e.g., via averaging) [49]. Such tools are suitable for relatively small disturbances, e.g., as shown in [50], [51]. Thus, small-signal modeling is considered here, where, each variable x is written as $x = x^{\mathrm{q}} + \hat{x}$, where x^{q} and $\hat{x}$ are the quiescent and small-signal perturbation parts, respectively. This representation helps to linearly express the droop voltage for the i–th converter, v_i^{d}, as

$$v_i^{\mathrm{d}} = v_i^{\mathrm{d,q}} + \hat{v}_i^{\mathrm{d}} = \left(r_i^{\mathrm{q}} + \hat{r}_i\right)\left(i_i^{\mathrm{q}} + \hat{i}_i\right). \tag{10}$$

By neglecting the second-order term, i.e., $\hat{r}_i\hat{i}_i \approx 0$, (10) can be reduced to

$$\hat{v}_i^{\mathrm{d}} = r_i^{\mathrm{q}}\hat{i}_i + i_i^{\mathrm{q}}\hat{r}_i. \tag{11}$$

Let $\hat{\mathbf{v}}_{\mathrm{ref}} = [\hat{v}_1^{\mathrm{ref}}, \hat{v}_2^{\mathrm{ref}}, \ldots, \hat{v}_N^{\mathrm{ref}}]^{\mathrm{T}}$ and $\hat{\mathbf{i}} = [\hat{i}_1, \hat{i}_2, \ldots, \hat{i}_N]^{\mathrm{T}}$ be the small-signal vectors of the rated voltages and actual supplied currents, respectively. Similarly, $\hat{\mathbf{v}}$, $\hat{\mathbf{v}}^{\mathrm{d}}$, $\Delta\hat{\mathbf{v}}$, $\hat{\mathbf{r}}$, and $\hat{\mathbf{v}}^*$ are column vectors containing small-signal portions of the output voltages, droop voltages, voltage correction terms, virtual impedances, and local voltage set points, respectively. $\mathbf{r}^{\mathrm{q}}$ and $\mathbf{i}^{\mathrm{q}}$ are vectors of quiescent virtual impedances and currents, respectively. $\mathbf{I}_{\mathrm{rated}} = \mathrm{diag}\{I_i^{\mathrm{rated}}\}$ is a diagonal matrix containing rated currents of individual sources. $\hat{\mathbf{V}}_{\mathrm{ref}}$, $\hat{\mathbf{I}}$, $\hat{\mathbf{V}}$, $\hat{\mathbf{V}}^{\mathrm{d}}$, $\Delta\hat{\mathbf{V}}$, $\hat{\mathbf{R}}$, and $\hat{\mathbf{V}}^*$ are the Laplace transforms of $\hat{\mathbf{v}}_{\mathrm{ref}}$, $\hat{\mathbf{i}}$, $\hat{\mathbf{v}}$, $\hat{\mathbf{v}}^{\mathrm{d}}$, $\Delta\hat{\mathbf{v}}$, $\hat{\mathbf{r}}$, and $\hat{\mathbf{v}}^*$, respectively. Based on Fig. 2,

$$\mathbf{H}\left(\hat{\mathbf{V}}_{\mathrm{ref}} - \hat{\overline{\mathbf{V}}}\right) = \Delta\hat{\mathbf{V}}, \tag{12}$$

where $\mathbf{H} = \mathrm{diag}\{H_i(s)\}$ is the voltage controller matrix. By using (3), $\hat{r}_i = -\delta\hat{r}_i$, thus,

$$-b\mathbf{G}\mathbf{L}\mathbf{I}_{\mathrm{rated}}^{-1}\hat{\mathbf{I}} = -\hat{\mathbf{R}}, \tag{13}$$

where $\mathbf{G} = \mathrm{diag}\{G_i(s)\}$ is the current controller matrix. Substituting the observer transfer function, $\mathbf{H}_{\mathrm{obs}}$, from (8) in (12) yields,

$$\Delta\hat{\mathbf{V}} = \mathbf{H}\left(\hat{\mathbf{V}}_{\mathrm{ref}} - \mathbf{H}_{\mathrm{obs}}\hat{\mathbf{V}}\right). \tag{14}$$

In addition, (11) can be written in the global form,

$$\hat{\mathbf{V}}^{\mathrm{d}} = \mathrm{T}\left(\mathbf{r}^{\mathrm{q}}\right)\hat{\mathbf{I}} + \mathrm{T}\left(\mathbf{i}^{\mathrm{q}}\right)\hat{\mathbf{R}}, \tag{15}$$

where $\mathrm{T}(\cdot){:}\mathbb{R}^{N\times 1} \to \mathbb{R}^{N\times N}$ is a transformation that maps a vector to a diagonal matrix,

$$\mathrm{T}\left([x_1, x_2, \cdots, x_N]^{\mathrm{T}}\right) \triangleq \mathrm{diag}\{x_1, x_2, \cdots, x_N\}. \tag{16}$$

The small-signal reference voltage vector, $\hat{\mathbf{V}}^*$, can be derived using (1) and (13)-(15),

$$\begin{aligned}\hat{\mathbf{V}}^{*} &= \hat{\mathbf{V}}_{\text{ref}} - \hat{\mathbf{V}}^{\text{d}} + \Delta\hat{\mathbf{V}} \\ &= \hat{\mathbf{V}}_{\text{ref}} - \mathrm{T}\left(\mathbf{r}^{\text{q}}\right)\hat{\mathbf{I}} - \mathrm{T}\left(\mathbf{i}^{\text{q}}\right)\hat{\mathbf{R}} + \mathbf{H}\left(\hat{\mathbf{V}}_{\text{ref}} - \mathbf{H}_{\text{obs}}\hat{\mathbf{V}}\right) \\ &= \left(\mathbf{I}_{N} + \mathbf{H}\right)\hat{\mathbf{V}}_{\text{ref}} - \left(\mathrm{T}\left(\mathbf{r}^{\text{q}}\right) + b\mathrm{T}\left(\mathbf{i}^{\text{q}}\right)\mathbf{GLI}_{\text{rated}}^{-1}\right)\hat{\mathbf{I}} \\ &\quad -\mathbf{HH}_{\text{obs}}\hat{\mathbf{V}}.\end{aligned} \tag{17}$$

On the other hand, dynamic behavior of any converter with closed-loop voltage regulator can be expressed as

$$\hat{V}_{i} = G_{i}^{\text{c}}(s)\hat{V}_{i}^{*}, \tag{18}$$

where $\hat{V}_i$ and $\hat{V}_i^*$ are the Laplace transforms of $\hat{v}_i$ and $\hat{v}_i^*$, respectively. G_i^{c} is the closed-loop transfer function of the $i-$th converter. The closed-loop transfer functions are derived in [49] for a wide variety of converters. Global small-signal dynamic of the converters can be found according to (18),

$$\hat{\mathbf{V}} = \mathbf{G}_{\text{c}}\hat{\mathbf{V}}^{*}, \tag{19}$$

where $\mathbf{G}_{\text{c}} = \text{diag}\{G_i^{\text{c}}\}$ is the converters' transfer function matrix. By substituting (19) in (17),

$$\begin{aligned}&\left(\mathbf{G}_{\text{c}}^{-1} + \mathbf{HH}_{\text{obs}}\right)\hat{\mathbf{V}} = \\ &\qquad\left(\mathbf{I}_{N} + \mathbf{H}\right)\hat{\mathbf{V}}_{\text{ref}} - \left(\mathrm{T}\left(\mathbf{r}^{\text{q}}\right) + b\mathrm{T}\left(\mathbf{i}^{\text{q}}\right)\mathbf{GLI}_{\text{rated}}^{-1}\right)\hat{\mathbf{I}}.\end{aligned} \tag{20}$$

For a dc Microgrid, it is a common practice to assume that the transmission/distribution line and load impedances are predominantly resistive [52]. Accordingly, one can use the Microgrid conductance matrix, $\mathbf{g}_{\text{bus}}$, to relate supplied currents to the bus voltages,

$$\mathbf{i} = \mathbf{g}_{\text{bus}}\mathbf{v}. \tag{21}$$

Small-signal perturbation expands (21),

$$\left(\mathbf{i}^{\text{q}} + \hat{\mathbf{i}}\right) = \left(\mathbf{g}_{\text{bus}}^{\text{q}} + \hat{\mathbf{g}}_{\text{bus}}\right)\left(\mathbf{v}^{\text{q}} + \hat{\mathbf{v}}\right). \tag{22}$$

The small-signal portion of the conductance matrix, $\hat{\mathbf{g}}_{\text{bus}}$, models any small-signal changes in the conductance matrix, $\mathbf{g}_{\text{bus}}$, caused by load change or transmission network reconfiguration. Neglecting the second-order term, i.e., $\hat{\mathbf{g}}_{\text{bus}}\hat{\mathbf{v}} \approx \mathbf{0}$, simplifies (22),

$$\hat{\mathbf{i}} = \mathbf{g}_{\text{bus}}^{\text{q}}\hat{\mathbf{v}} + \hat{\mathbf{g}}_{\text{bus}}\mathbf{v}^{\text{q}}. \tag{23}$$

Or, equivalently, in the frequency domain,

$$\hat{\mathbf{I}} = \mathbf{g}_{\text{bus}}^{\text{q}}\hat{\mathbf{V}} + \hat{\mathbf{G}}_{\text{bus}}\mathbf{v}^{\text{q}}. \tag{24}$$

where $\hat{\mathbf{G}}_{\text{bus}}$ is the Laplace transform of $\hat{\mathbf{g}}_{\text{bus}}$. Substituting (24) in (20) provides the global dynamic model of the Microgrid with the proposed controller in effect,

$$\begin{aligned}&\left(\mathbf{G}_{\text{c}}^{-1} + \mathbf{HH}_{\text{obs}} + \left(\mathrm{T}\left(\mathbf{r}^{\text{q}}\right) + b\mathrm{T}\left(\mathbf{i}^{\text{q}}\right)\mathbf{GLI}_{\text{rated}}^{-1}\right)\mathbf{g}_{\text{bus}}^{\text{q}}\right)\hat{\mathbf{V}} = \\ &\qquad\left(\mathbf{I}_{N} + \mathbf{H}\right)\hat{\mathbf{V}}_{\text{ref}} - \left(\mathrm{T}\left(\mathbf{r}^{\text{q}}\right) + b\mathrm{T}\left(\mathbf{i}^{\text{q}}\right)\mathbf{GLI}_{\text{rated}}^{-1}\right)\hat{\mathbf{G}}_{\text{bus}}\mathbf{v}^{\text{q}}.\end{aligned} \tag{25}$$

Equation (25) implies that the Microgrid is systematically a multi-input-multi-output plant where $\hat{\mathbf{V}}^{\text{ref}}$ and $\hat{\mathbf{G}}_{\text{bus}}$ are the inputs and $\hat{\mathbf{V}}$ and $\hat{\mathbf{I}}$ are the outputs. The global dynamic model in (25) formulates the transfer functions from each input to the primary output, $\hat{\mathbf{V}}$.

B. Design Approach

For a given Microgrid, the matrix of converters' closed-loop transfer functions, $\mathbf{G}_{\text{c}}$, and the current rating matrix, $\mathbf{I}_{\text{rated}}$ are known. The communication graph needs to be a connected graph with the minimal redundancy defined in Section III, where no single link failure can compromise communication connectivity. Weights of the communication links, a_{ij}, and, thus, the Laplacian matrix, $\mathbf{L}$, may, then, be chosen to provide any desired dynamic response for the voltage observers by evaluating (8). It should be noted that the selection of the communication weights must satisfy a balanced Laplacian matrix.

For the given Microgrid with known transmission/ distribution network, one can evaluate $\mathbf{g}_{\text{bus}}^{\text{q}}$ assuming base loads at all consumption terminals. Accordingly, quiescent voltage and current vectors ($\mathbf{v}^{\text{q}}$ and $\mathbf{i}^{\text{q}}$, respectively) can be found by iteratively solving (26)-(27),

$$\mathbf{i}^{\text{q}} = \mathbf{g}_{\text{bus}}^{\text{q}}\mathbf{v}^{\text{q}}, \tag{26}$$

$$\mathbf{i}^{\text{pu}^{\text{q}}} = \mathbf{I}_{\text{rated}}^{-1}\mathbf{i}^{\text{q}} = n\underline{\mathbf{1}}, \tag{27}$$

where n is a positive real number. The designer may initialize the virtual impedances as

$$\mathbf{r}_{0} = m\left[1/I_{1}^{\text{rated}}, 1/I_{2}^{\text{rated}}, \cdots, 1/I_{N}^{\text{rated}}\right]^{\text{T}}, \tag{28}$$

where m is a positive scalar design parameter [7]. The adaptive-droop mechanism adjusts the virtual impedances to provide proportional load sharing. Due to the line impedances, this adjustment results in different values than the initial values, i.e., $\mathbf{r}^{\text{q}} \neq \mathbf{r}_{0}$. However, empirical studies in Section VI will show that the quiescent virtual impedance vector remains almost intact for various operating conditions. Thus, one can run a steady-state numerical analysis to find $\mathbf{r}^{\text{q}}$ for the base load condition and further use it in the design procedure.

Given the Laplacian matrix, $\mathbf{L}$, the observer transfer function, $\mathbf{H}_{\text{obs}}$, the converters' transfer function matrix, $\mathbf{G}_{\text{c}}$, and all other constant vectors in (25), one can use this equation to design the voltage and current controller matrices ($\mathbf{H}$ and $\mathbf{G}$, respectively) and the coupling gain, b, to provide any desired asymptotically stable dynamic response for the entire Microgrid, where all poles of the transfer functions extracted from (25) lie on the Open Left Hand Plane (OLHP).

C. Steady-State Analysis

Steady-state analysis of the Microgrid operation is essential to ensure that the cooperative controllers satisfy both operational requirements; the global voltage regulation and the proportional load sharing. Since the converters' rated voltages match the Microgrid rated voltage, with no loss of generality, one can assume

$$\mathbf{v}_{\text{ref}} = v_{\text{rated}}\underline{\mathbf{1}}, \tag{29}$$

where v_{rated} is the Microgrid rated voltage. It is also assumed that the control parameters are properly tuned, based on the design approach in Section V-B, to stabilize voltage and current throughout the Microgrid.

Let's assume that the Microgrid voltages and currents are in the steady state for $t \geq t_0$. The voltage and current controller of the i–th converter can be expressed as $H_i = H_i^{\mathrm{P}} + H_i^{\mathrm{I}}/s$ and $G_i = G_i^{\mathrm{P}} + G_i^{\mathrm{I}}/s$, respectively, where H_i^{P} and G_i^{P} are the proportional and H_i^{I} and G_i^{I} are the integral gains. One can show that, with stable voltages, all voltage observers converge to the true average voltage, i.e.,

$$\overline{\mathbf{v}}^{\mathrm{ss}} = \left(\frac{1}{N}\sum_{i=1}^{N} v_i^{\mathrm{ss}}\right)\underline{\mathbf{1}} = \overline{v}^{\mathrm{ss}}\underline{\mathbf{1}}, \tag{30}$$

where x^{ss} represents the steady-state value of the variable x. According to Fig. 2, for $t \geq t_0$ one can write,

$$\begin{aligned}\Delta\mathbf{v}^{\mathrm{ss}} = \mathbf{W}_{\mathbf{v}}(t_0) + \mathbf{H}_{\mathrm{P}}(\mathbf{v}_{\mathrm{ref}} - \overline{\mathbf{v}}^{\mathrm{ss}}) \\ + \mathbf{H}_{\mathrm{I}}(\mathbf{v}_{\mathrm{ref}} - \overline{\mathbf{v}}^{\mathrm{ss}})(t - t_0),\end{aligned} \tag{31}$$

where $\mathbf{W}_{\mathbf{v}}(t_0)$ is a vector that carries integrator outputs of the voltage regulators at $t = t_0$. Similarly,

$$\begin{aligned}\Delta\mathbf{r}^{\mathrm{ss}} = \mathbf{W}_{\mathbf{r}}(t_0) + \mathbf{G}_{\mathrm{P}}(-b\mathbf{L}\mathbf{i}^{\mathrm{pu}^{\mathrm{ss}}}) \\ + \mathbf{G}_{\mathrm{I}}(-b\mathbf{L}\mathbf{i}^{\mathrm{pu}^{\mathrm{ss}}})(t - t_0),\end{aligned} \tag{32}$$

where $\mathbf{W}_{\mathbf{r}}(t_0)$ is a vector that carries integrator outputs of the current regulators at $t = t_0$. In the steady state, $\mathbf{v}^{\mathrm{ss}} = \mathbf{v}^{*^{\mathrm{ss}}}$, thus, according to (1),

$$\begin{aligned}\mathbf{v}^{\mathrm{ss}} &= \mathbf{v}_{\mathrm{ref}} - \mathrm{T}\left(\mathbf{r}^{\mathrm{ss}}\right)\mathbf{i}^{\mathrm{ss}} + \Delta\mathbf{v}^{\mathrm{ss}} \\ &= v_{\mathrm{rated}}\underline{\mathbf{1}} - \mathrm{T}\left(\mathbf{r}_0 - \Delta\mathbf{r}^{\mathrm{ss}}\right)\mathbf{i}^{\mathrm{ss}} + \Delta\mathbf{v}^{\mathrm{ss}}.\end{aligned} \tag{33}$$

By substituting (31)-(32) in (33),

$$\begin{aligned}\mathbf{v}^{\mathrm{ss}} &= v_{\mathrm{rated}}\underline{\mathbf{1}} \\ &-\mathrm{T}\left(\mathbf{r}_0 + b\left(\mathbf{G}_{\mathrm{P}} + \mathbf{G}_{\mathrm{I}}(t-t_0)\right)\mathbf{L}\mathbf{i}^{\mathrm{pu}^{\mathrm{ss}}} - \mathbf{W}_{\mathbf{r}}(t_0)\right)\mathbf{i}^{\mathrm{ss}} \\ &+\left(v_{\mathrm{rated}} - \overline{v}^{\mathrm{ss}}\right)\left(\mathbf{H}_{\mathrm{P}} + \mathbf{H}_{\mathrm{I}}(t-t_0)\right)\underline{\mathbf{1}} + \mathbf{W}_{\mathbf{v}}(t_0).\end{aligned} \tag{34}$$

Equation (34) holds for all $t \geq t_0$. Thus, the time varying term in (34) is zero. Accordingly,

$$\left(v_{\mathrm{rated}} - \overline{v}^{\mathrm{ss}}\right)\mathbf{H}_{\mathrm{I}}\underline{\mathbf{1}} = \mathrm{T}\left(b\mathbf{G}_{\mathrm{I}}\mathbf{L}\mathbf{i}^{\mathrm{pu}^{\mathrm{ss}}}\right)\mathbf{i}^{\mathrm{ss}}. \tag{35}$$

One can see that if $\mathbf{G}$ is a diagonal matrix and b a real number then, for any vector $\mathbf{x}$,

$$\mathrm{T}\left(b\mathbf{G}\mathbf{x}\right) = b\mathbf{G}\mathrm{T}\left(\mathbf{x}\right). \tag{36}$$

The transformation property in (36) helps to rewrite (35),

$$\mathrm{T}\left(\mathbf{L}\mathbf{i}^{\mathrm{pu}^{\mathrm{ss}}}\right)\mathbf{I}_{\mathrm{rated}}\mathbf{i}^{\mathrm{pu}^{\mathrm{ss}}} = \left(v_{\mathrm{rated}} - \overline{v}^{\mathrm{ss}}\right)b^{-1}\mathbf{G}_{\mathrm{I}}^{-1}\mathbf{H}_{\mathrm{I}}\underline{\mathbf{1}}. \tag{37}$$

Both $\mathrm{T}(\mathbf{L}\mathbf{i}^{\mathrm{pu}^{\mathrm{ss}}})$ and $\mathbf{I}_{\mathrm{rated}}$ are diagonal matrices and, thus,

$$\mathrm{T}\left(\mathbf{L}\mathbf{i}^{\mathrm{pu}^{\mathrm{ss}}}\right)\mathbf{I}_{\mathrm{rated}} = \mathbf{I}_{\mathrm{rated}}\mathrm{T}\left(\mathbf{L}\mathbf{i}^{\mathrm{pu}^{\mathrm{ss}}}\right). \tag{38}$$

Accordingly,

$$\begin{aligned}\mathrm{T}\left(\mathbf{L}\mathbf{i}^{\mathrm{pu}^{\mathrm{ss}}}\right)\mathbf{i}^{\mathrm{pu}^{\mathrm{ss}}} &= \left(v_{\mathrm{rated}} - \overline{v}^{\mathrm{ss}}\right)b^{-1}\mathbf{I}_{\mathrm{rated}}^{-1}\mathbf{G}_{\mathrm{I}}^{-1}\mathbf{H}_{\mathrm{I}}\underline{\mathbf{1}} \\ &= \left(v_{\mathrm{rated}} - \overline{v}^{\mathrm{ss}}\right)\left[u_1, u_2, \cdots, u_N\right]^{\mathrm{T}}.\end{aligned} \tag{39}$$

where $u_i = H_i^{\mathrm{I}}/(bG_i^{\mathrm{I}}I_i^{\mathrm{rated}}) > 0$. If any of the currents is zero, e.g., $i_j^{\mathrm{pu}} = 0$, then, (39) implies $v_{\mathrm{rated}} = \overline{v}^{\mathrm{ss}}$.

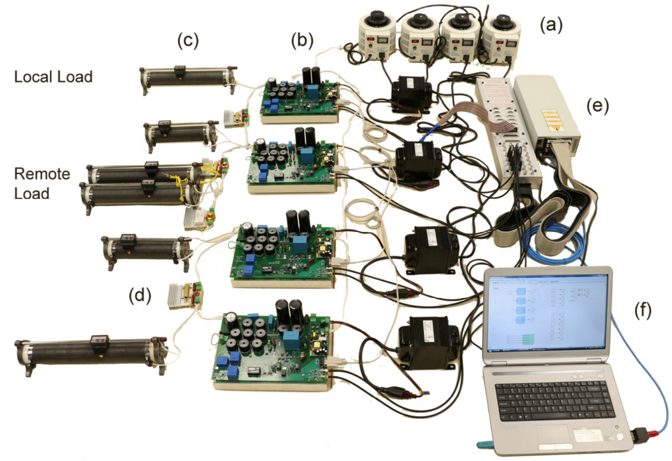

Fig. 4. DC Microgrid prototype: (a) Input ac sources, (b) Buck converters driving each source, (c) Local and remote loads, (d) distribution line, (e) dSAPCE control board (DS1103), (f) Programming/monitoring PC.

Otherwise, one can safely assume that all currents are positive (i.e., $i_i > 0$); sources only deliver power. Using (39),

$$\mathbf{L}\mathbf{i}^{\mathrm{pu}^{\mathrm{ss}}} = \left(v_{\mathrm{rated}} - \overline{v}^{\mathrm{ss}}\right)\left[\frac{u_1}{i_1^{\mathrm{pu}}}, \frac{u_2}{i_2^{\mathrm{pu}}}, \cdots, \frac{u_N}{i_N^{\mathrm{pu}}}\right]^{\mathrm{T}}. \tag{40}$$

with the balanced Laplacian matrix, $\mathbf{L}$,

$$\underbrace{\underline{\mathbf{1}}^{\mathrm{T}}\mathbf{L}}_{=0}\mathbf{i}^{\mathrm{pu}^{\mathrm{ss}}} = \left(v_{\mathrm{rated}} - \overline{v}^{\mathrm{ss}}\right)\underbrace{\sum_{j=1}^{N}\frac{u_j}{i_j^{\mathrm{pu}}}}_{>0}. \tag{41}$$

Accordingly,

$$v_{\mathrm{rated}} = \overline{v}^{\mathrm{ss}}, \tag{42}$$

which, equivalently, satisfies the global voltage regulation, i.e., the controller successfully regulates the average voltage of the Microgrid, $\overline{v}^{\mathrm{ss}}$, at the rated value, v_{rated}.

For any vector $\mathbf{x}$ one can investigate that

$$\underline{\mathbf{1}}^{\mathrm{T}}\mathrm{T}(\mathbf{x}) = \mathbf{x}^{\mathrm{T}}. \tag{43}$$

Multiplying both sides of (39) from left by $\underline{\mathbf{1}}^{\mathrm{T}}$, one can write

$$\left(\mathbf{i}^{\mathrm{pu}^{\mathrm{ss}}}\right)^{\mathrm{T}}\mathbf{L}^{\mathrm{T}}\mathbf{i}^{\mathrm{pu}^{\mathrm{ss}}} = \left(v_{\mathrm{rated}} - \overline{v}^{\mathrm{ss}}\right)\sum_{j=1}^{N}u_j = 0, \tag{44}$$

which is a quadratic equation. It is shown in Appendix I that

$$\mathbf{i}^{\mathrm{pu}^{\mathrm{ss}}} = k\underline{\mathbf{1}}, \tag{45}$$

is the only solution to the quadratic equation in (44), where k is a positive real number. Equation (45) ensures consensus of the per-unit currents or, equivalently, achievement of proportional load sharing.

VI. Experimental Verification

A low-voltage dc Microgrid, with the structure shown in Fig. 1, is prototyped. Figure 4 shows the test bench where four adjustable isolated ac sources are used as energy sources. Each source is driven by a buck converter with an input rectifier.

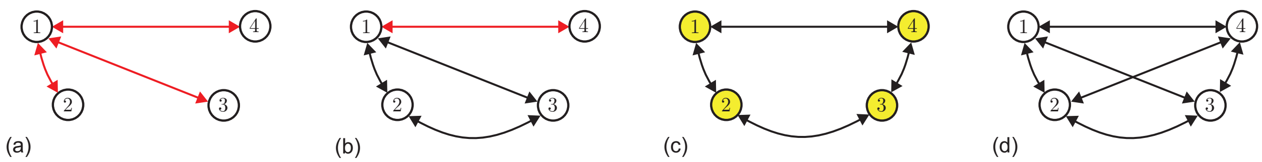

Fig. 5. Alternative communication topologies forming a connected graph with: (a) No redundant link, (b) Suboptimal link redundancy, (c) Optimal link redundancy, and (d) full connection.

The converters have similar topologies but different ratings, i.e., the rated currents of the first and the fourth converters are twice those for the other two converters. Each distribution line is built using a π–circuit model. The Microgrid has five consumption terminals; four to supply local loads and one to supply a remote load, as seen in Fig. 1. Although different voltage levels are possible [53], [54], a $48\ \mathrm{V}$ system is considered here. The typical acceptable voltage deviation is about 5% of the rated voltage [22] and, thus, the voltage limiters are set with $\varepsilon = 2.5\ \mathrm{V}$. Electrical and control parameters of the Microgrid are provided in Appendix II.

Alternative communication topologies for a group of four agents are represented in Fig. 5, where all links are assumed bidirectional to feature a balanced Laplacian matrix. Despite carrying spanning tree, not all alternatives satisfy the communication redundancy required for the safe operation (link failure resiliency) of the proposed method. In other words, some topologies are susceptible to lose connectivity in the case of a single link failure. For example, if any of the links highlighted in red in Figs. 5(a) or 5(b) is lost, the corresponding graph losses its connectivity, which renders the whole control mechanism inoperable. However, the circular communication structure in Fig. 5(c) is the sparsest network where no single link failure can compromise the graphical connectivity. Figure 5(d) shows a fully connected graph, which provides a similar redundancy feature yet lacks sparsity. Therefore, the communication structure in Fig. 5(c) is considered for this study.

The communication channels are assumed ideal and are modeled in the dSAPCE. Wireless or fiber optic networks may be used for physical implementation of the data network. The effect of non-idealities such as noise, limited bandwidth, channel delay, packet drop, etc. is studied in [45]. Moreover, consensus protocols are tailored for non-ideal data networks in [55]–[57], whose application in the power distribution systems will be the subject of future studies.

The control approach is built in Simulink on a programming/monitoring PC which is linked to a dSPACE control board (DS1103). The PC compiles the Simulink model and, accordingly, programs the DS1103. It also generates a variable description file further used by the dSPACE monitoring software, ControlDesk 5.0, to provide a live view of any variable. When the proposed control methodology is in effect, the ControlDesk enables the designer to tune any control parameter online and monitor the system performance.

A. Constant Droop versus Adaptive Droop

Figure 6 comparatively studies the performance of the proposed methodology. The Microgrid is initially controlled using the conventional droop controller, where a fixed droop impedance is used, i.e., $\mathbf{r}(t) = \mathbf{r}_0$. As seen in Fig. 6(a), it leads to voltages less than the desired value, i.e., $v_{\mathrm{rated}} = 48\ \mathrm{V}$. In addition, although the initial values of the droop gains are designed reciprocal to the converters' rated currents, the transmission line effect has clearly incapacitated the droop mechanism, resulting in a poor load sharing where converters with identical ratings supply different currents (see Fig. 6(b)). The proposed controller is engaged at $t = 10.1\ \mathrm{s}$. Consequently, the voltages are boosted across the Microgrid and the average voltage is finely regulated at the set point, i.e., $v_{\mathrm{rated}} = 48\ \mathrm{V}$. Figure 6(b) shows that the proportional load sharing is also carried out, where the first and the fourth converters carry twice the current as the other two converters. Dynamic performance of the controller can be tuned by adjusting the communication weights (or, equivalently, entries of the Adjacency matrix). In comparison with alternative solution in [46], it can be seen that the distributed adaptive droop has provided a faster load sharing; almost twice as fast as the method in [46].

The voltage observers is studied in Fig. 6(c), where a good agreement is reported between the true average voltage, $\overline{v}$, and the individual estimated values, $\overline{v}_i$ s. Figure 6(d) expresses how the proposed controller sets voltage correction terms, δv_i s, to boost the voltage across the Microgrid and overcome the natural voltage drop caused by the droop mechanisms. Figure 6(e) shows how the current controller adjusts the virtual impedances, r_i s, to provide proportional load sharing.

B. Load Variation

The controller performance in case of load change is studied in Fig. 7, where the remote load at bus five, R_5, is changed in step between 10Ω and 20Ω. Tight voltage regulation and load sharing can be observed in Figs. 7(a) and 7(b). Excellent transient load sharing is also noticeable in Fig. 7(b). Estimations of the average voltage across the Microgrid are plotted in Fig 7(c) where a good agreement between the true and estimated values ($\overline{v}$ and $\overline{v}_i$ s, respectively) can be seen. Comparing Figs. 7(d) and 7(e), one can observe that load change mostly affects voltage correction terms, δv_i s, and has a negligible impact on the virtual impedances.

C. Plug-and-Play Capability

Figure 8 studies plug-and-play capability of the proposed method and its performance in the case of a converter failure. As seen, when the second converter fails at $t = 7.3\ \mathrm{s}$, the controller adjusts the voltages to regain the global voltage regulation. When the Converter 2 fails, the voltage at the second bus, v_2, is no longer available.

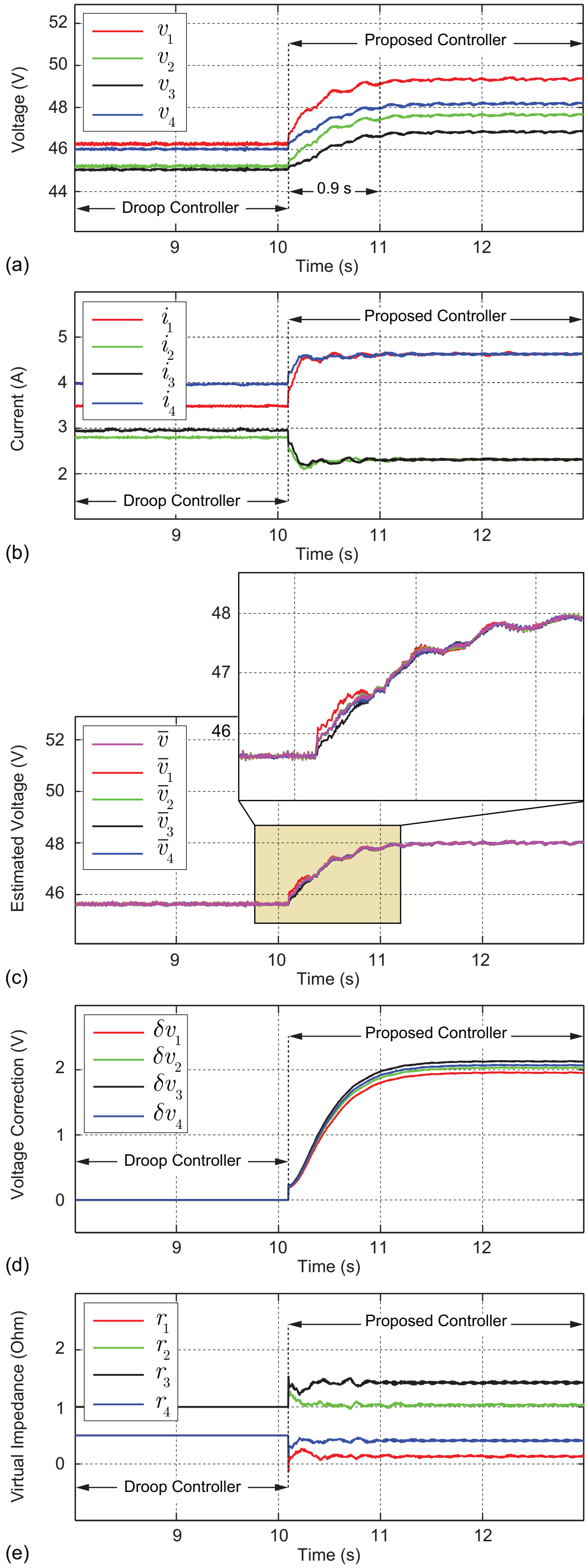

Fig. 6. Comparative studies of the conventional droop control and the distributed adaptive-droop control: (a) Terminal voltages, (b) Supplied currents, (c) Estimations of the average voltage, (d) Voltage correction terms, (e) Virtual impedances.

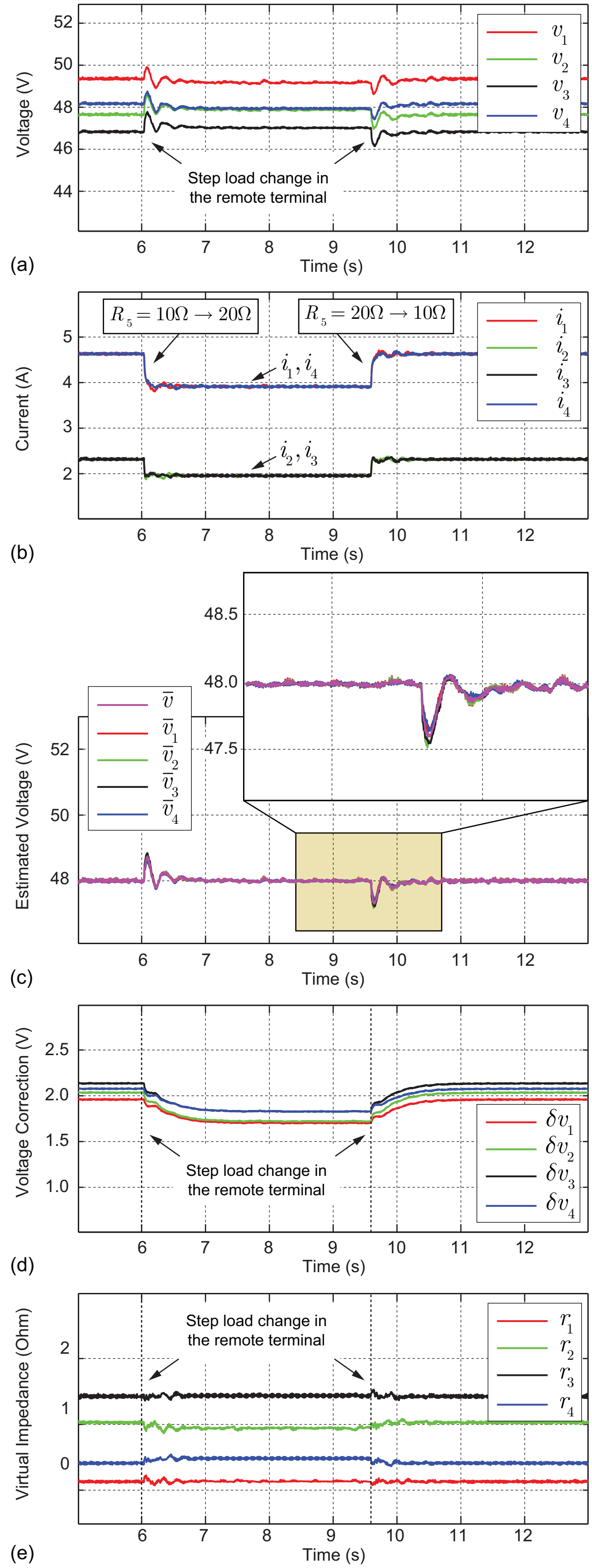

Fig. 7. Performance of the distributed adaptive-droop controller in a case of load change: (a) Terminal voltages, (b) Supplied currents, (c) Estimations of the average voltage, (d) Voltage correction terms, (e) Virtual impedances.

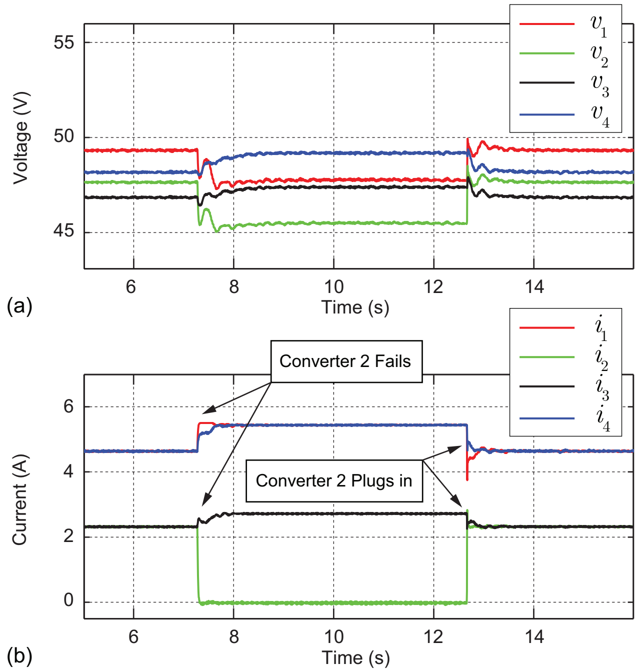

Fig. 8. Converter failure and plug-and-play studies: (a) Terminal voltages, (b) Supplied currents.

Thus, the controller averages the three remaining measurements, i.e., v_1, v_3, and v_4, and regulates this new average at the reference value. The controller also readjusts the load sharing among the remaining converters. It should be noted that a converter failure also implies loss of all communication links attached to that particular converter. Accordingly, failure of the second converter automatically renders the link 1-2 (between nodes 1 and 2) and link 2-3 inoperable. However, the remaining links still form a connected graph with balanced Laplacian matrix (see Fig. 1, cyber layer) and, thus, the whole control system is still functional. Then, the Converter 2 is plugged back at $t = 12.6$ s. As seen, the controller has properly updated the load sharing and global voltage regulation, afterwards.

D. Link-failure Resiliency

Resiliency to a single link failure is studied next in Fig. 9. The original communication graph in Fig. 1 is designed to carry a minimal redundancy, so no single link failure can cause loss of connectivity in the graph. Thus, the control system shall remain operational. As seen in Fig. 9, the link 1-2 has failed at $t = 4.0$ s, but it does not have any impact on voltage regulation or load sharing. Controller response to the step load change in the remote load is also studied with the failed link, where a satisfactory performance can be seen. It should be noted that the reconfiguration caused by the link failure affects the Laplacian matrix and, thus, the whole system dynamic but not the steady-state performance.

Generally, any link failure limits information flow and can slightly slow down the transient response. Similar to Fig. 7(e), Fig. 9(d) demonstrates negligible impact of load change on the virtual impedances. However, by comparison, Fig. 7(e) shows more stable impedances than those of Fig. 9(d).

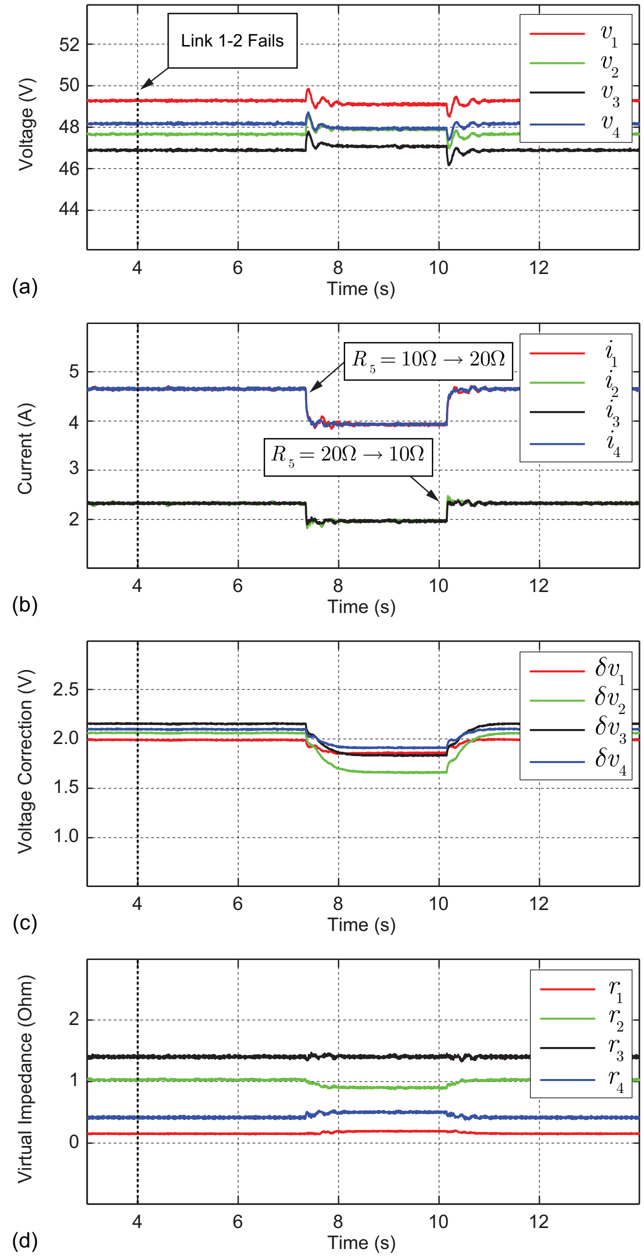

Fig. 9. Link-failure resiliency: (a) Terminal voltages, (b) Supplied currents, (c) Voltage correction terms, (d) Virtual impedances.

This observation concludes that higher graphical connectivity results in more stable droop impedances. In addition, small variations of the virtual impedance terms in Figs. 7(e) and 9(d) implies that the developed small-signal model in Section V-A is appropriate for modeling and stability analysis of the proposed adaptive droop mechanism.

VII. Conclusion

An adaptive droop-based distributed secondary controller is proposed for dc Microgrids. The controller on each converter comprises two modules; the voltage regulator and the current regulator. The voltage regulator uses a cooperative voltage observer to estimate the global average voltage. This estimation is then further used to boost the local voltage set point to provide global voltage regulation. The current regulator at each source compares local per-unit current with its neighbors' and, accordingly, adjusts the local virtual impedance to carry out proportional load sharing. This control paradigm uses a sparse communication network for data exchange among converters. Studies show that the proposed cooperative control provides precise global voltage regulation and proportional load sharing. Plug-and-play capability and link-failure resiliency of the control structure are also verified through experiments. It is also discussed that the droop coefficients show slight variations in response to load variations, which makes the small-signal modeling a viable approach for stability analysis of the proposed controller.

Future works focus on two main areas: 1) Study of alternative communication infrastructures, effects of channel non-idealities (e.g., delay or packet drop), and, consequently, to tailor consensus protocols to account for non-ideal data network; 2) Development of distributed optimization techniques for cost optimization in the tertiary control level.

APPENDIX I: SOLUTION TO THE QUADRATIC EQUATION

Theorem A.1: Assume $\mathbf{L}$ is the Laplacian matrix of a communication graph with at least one spanning tree. If $\mathbf{L}$ is balanced then, the only solution to the quadratic equation $\mathbf{x}^{\mathrm{T}}\mathbf{L}\mathbf{x} = 0$ is $\mathbf{x} = k\underline{\mathbf{1}}$, where k is a real number.

Proof: The quadratic form, $\mathbf{x}^{\mathrm{T}}\mathbf{L}\mathbf{x}$, is a real number. Thus,

$$\mathbf{x}^{\mathrm{T}}\mathbf{L}\mathbf{x} = \left(\mathbf{x}^{\mathrm{T}}\mathbf{L}\mathbf{x}\right)^{\mathrm{T}} = \mathbf{x}^{\mathrm{T}}\mathbf{L}^{\mathrm{T}}\mathbf{x} = \mathbf{x}^{\mathrm{T}}\left(\frac{\mathbf{L}+\mathbf{L}^{\mathrm{T}}}{2}\right)\mathbf{x}. \tag{A.1}$$

Let's define the co-Laplacian matrix as $\mathbf{L}_{\mathrm{c}} \triangleq \left(\mathbf{L}+\mathbf{L}^{\mathrm{T}}\right)/2$, which is a symmetric matrix. Assume $\mathbf{L} = [l_{ij}] \in \mathbb{R}^{N\times N}$ and $\mathbf{L}_{\mathrm{c}} = [l_{ij}^{\mathrm{c}}] \in \mathbb{R}^{N\times N}$. Then,

$$\begin{cases} l_{ii}^{\mathrm{c}} = 2l_{ii} \geq 0, \\ l_{ij}^{\mathrm{c}} = l_{ij} + l_{ji} = l_{ji}^{\mathrm{c}} \leq 0, \qquad i \neq j \end{cases} \tag{A.2}$$

Since the Laplacian matrix, $\mathbf{L}$, is balanced,

$$l_{ii} = -\sum_{j\in N_i} l_{ij} = -\sum_{j=1(j\neq i)}^{N} l_{ij} = -\sum_{j=1(j\neq i)}^{N} l_{ji}. \tag{A.3}$$

Accordingly, one can formulate diagonal elements of the co-Laplacian matrix, $\mathbf{L}_{\mathrm{c}}$,

$$l_{ii}^{\mathrm{c}} = -\sum_{j=1(j\neq i)}^{N}\left(l_{ij}+l_{ji}\right) = -\sum_{j=1(j\neq i)}^{N} l_{ij}^{\mathrm{c}} = -\sum_{j=1(j\neq i)}^{N} l_{ji}^{\mathrm{c}}. \tag{A.4}$$

The quadratic equation can be expanded using (A.4)

$$\begin{aligned}
\mathbf{x}^{\mathrm{T}}\mathbf{L}\mathbf{x} &= \frac{1}{2}\mathbf{x}^{\mathrm{T}}\mathbf{L}_{\mathrm{c}}\mathbf{x} = \frac{1}{2}\sum_{1\leq i,j\leq N} x_i l_{ij}^{\mathrm{c}} x_j \\
&= \frac{1}{2}\sum_{i=1}^{N} x_i^2 l_{ii}^{\mathrm{c}} + \frac{1}{2}\sum_{i\neq j} x_i l_{ij}^{\mathrm{c}} x_j \\
&= -\frac{1}{2}\sum_{i=1}^{N}\left(\sum_{j=1(j\neq i)}^{N} l_{ij}^{\mathrm{c}}\right)x_i^2 + \frac{1}{2}\sum_{i\neq j} x_i l_{ij}^{\mathrm{c}} x_j \\
&= \frac{1}{2}\sum_{i<j}\left(x_i l_{ij}^{\mathrm{c}} x_j - x_i^2 l_{ij}^{\mathrm{c}} - x_j^2 l_{ji}^{\mathrm{c}} + x_j l_{ji}^{\mathrm{c}} x_i\right) \\
&= -\frac{1}{2}\sum_{i<j} l_{ij}^{\mathrm{c}}\left(x_i - x_j\right)^2 = 0
\end{aligned} \tag{A.5}$$

where $\mathbf{x} = [x_1, x_2, \cdots, x_N]^{\mathrm{T}}$. All off-diagonal entries of the co-Laplacian matrix, $\mathbf{L}_{\mathrm{c}}$, are non-positive. Thus, (A.5) holds if and only if for every two connected nodes, i.e., $a_{ij} > 0$, $x_i = x_j$.

The communication graph has a spanning tree and, thus, has a root node, from which there exists a path to every other node. Assume that v_i^{g} is the root node then, for any other node, v_j^{g}, one can find a sequence of nodes connecting v_i^{g} to v_j^{g},

$$v_i^{\mathrm{g}} \to v_k^{\mathrm{g}} \to \cdots \to v_l^{\mathrm{g}} \to v_j^{\mathrm{g}}. \tag{A.6}$$

Given that for every two connected nodes associated entries of the vector $\mathbf{x}$ are equal, one can conclude

$$x_i = x_k = \cdots = x_l = x_j. \tag{A.7}$$

Thus, the vector $\mathbf{x}$ has equal entries, i.e., $\mathbf{x} = k\underline{\mathbf{1}}$, where k is a real number. ■

APPENDIX II

Each of the underlying buck converters has $L = 2640\ \mu\mathrm{H}$ and $C = 2.2\ \mathrm{mF}$ and operates with $F_s = 60\ \mathrm{kHz}$ switching frequency. Impedances of the transmission lines are $Z_{12} = Z_{34} = Z_b$ and $Z_{25} = Z_{35} = 2Z_b$, where the base impedance is $Z_b = 0.5 + (50\ \mu\mathrm{H})s$. Impedances of the local loads are $R_1 = 30\Omega$ and $R_2 = R_3 = R_4 = 20\Omega$. Voltages of the (rectified) input sources are $V_{\mathrm{s1}} = V_{\mathrm{s4}} = 100\,\mathrm{V}$ and $V_{\mathrm{s2}} = V_{\mathrm{s3}} = 80\,\mathrm{V}$. The control parameters are as follow,

$$\mathbf{I}_{\mathrm{rated}} = \mathrm{diag}\{6,3,3,6\}, \tag{A.8}$$

$$b = 0.5, \tag{A.9}$$

$$\mathbf{H}_{\mathrm{P}} = 0.1\times\mathbf{I}_4,\ \ \mathbf{H}_{\mathrm{I}} = 2.5\times\mathbf{I}_4, \tag{A.10}$$

$$\mathbf{G}_{\mathrm{P}} = 0.3\times\mathbf{I}_4,\ \ \mathbf{G}_{\mathrm{I}} = 5\times\mathbf{I}_4, \tag{A.11}$$

$$\mathbf{A}_{\mathbf{G}} = \begin{bmatrix} 0 & 10 & 0 & 10 \\ 10 & 0 & 10 & 0 \\ 0 & 10 & 0 & 10 \\ 10 & 0 & 10 & 0 \end{bmatrix},\ \ \mathbf{r}_0 = \begin{bmatrix} 0.5 & 0 & 0 & 0 \\ 0 & 1 & 0 & 0 \\ 0 & 0 & 1 & 0 \\ 0 & 0 & 0 & 0.5 \end{bmatrix}. \tag{A.12}$$

REFERENCES

[1] D. Chen and L. Xu, "Autonomous dc voltage control of a dc Microgrid with multiple slack terminals," *IEEE Trans. Power Syst.*, vol. 27, no. 4, pp. 1897–1905, Nov. 2012.

[2] M. Datta, T. Senjyu, A. Yona, T. Funabashi, and C. H. Kim, "A frequency-control approach by photovoltaic generator in a PV-diesel hybrid power system," *IEEE Trans. Energy Convers.*, vol. 26, no. 2, pp. 559–571, Jun. 2011.

[3] S. Teleke, M. E. Baran, A. Q. Huang, S. Bhattacharya, and L. Anderson, "Control strategies for battery energy storage for wind farm dispatching," *IEEE Trans. Energy Convers.*, vol. 24, no. 3, pp. 725–732, Sept. 2009.

[4] Y. K. Chen, Y. C. Wu, C. C. Song, and Y. S. Chen, "Design and implementation of energy management system with fuzzy control for dc Microgrid systems," *IEEE Trans. Power Electron.*, vol. 28, no. 4, pp. 1563–1570, Apr. 2013.

[5] A. Kwasinski and C, N. Onwuchekwa, “Dynamic behavior and stabilization of dc Microgrids with instantaneous constant-power loads,” *IEEE Trans. Power Electronics*, vol. 26, pp. 822-834, March 2011.

[6] R. S. Balog, W. Weaver, and P. T. Krein, “The load as an energy asset in a distributed dc Smartgrid architecture,” *IEEE Trans. Smart Grid*, vol. 3, pp. 253-260, March 2012.

[7] J. M. Guerrero, J. C. Vasquez, J. Matas, L. G. de Vincuña, and M. Castilla, “Hierarchical control of droop-controlled ac and dc Microgrids – a general approach toward standardization,” *IEEE Trans. Ind. Electron.*, vol. 58, pp. 158–172, Jan. 2011.

[8] M. Savaghebi, A. Jalilian, J. C. Vasquez, and J. M. Guerrero, “Secondary control scheme for voltage unbalance compensation in an islanded droop-controlled Microgrid,” *IEEE Trans. Smart Grid*, vol. 3, no. 2, pp. 797–807, Jun. 2012.

[9] X. Lu, J. M. Guerrero, K. Sun, J. C. Vasquez, R. Teodorescu, and L. Huang, “Hierarchical control of parallel ac-dc converter interfaces for hybrid Microgrids,” *IEEE Trans. Smart Grid*, vol. 5, pp. 683–692, Mar. 2014.

[10] C. Lin, P. Wang, J. Xiao, Y. Tang, and F. H. Choo, “Implementation of hierarchical control in dc Microgrids,” *IEEE Trans. Ind. Electron.*, vol. 61, pp. 4032–4042, Aug. 2014.

[11] L. Xu and D. Chen, “Control and operation of a dc Microgrid with variable generation and energy storage,” *IEEE Trans. Power Del.*, vol. 26, no. 4, pp. 2513–2522, Oct. 2011.

[12] H. Kanchev, D. Lu, F. Colas, V. Lazarov, and B. Francois, “Energy management and operational planning of a Microgrid with a PV-based active generator for smart grid applications,” *IEEE Trans. Ind. Electron*., vol. 58, no. 10, pp. 4583–4592, Oct. 2011.

[13] C. Chen, S. Duan, T. Cai, B. Liu, and G. Hu, “Optimal allocation and economic analysis of energy storage system in Microgrids,” *IEEE Trans. Power Electron*., vol. 26, no. 10, pp. 2762–2773, Oct. 2011.

[14] T. Zhou and B. Francois, “Energy management and power control of a hybrid active wind generator for distributed power generation and grid integration,” *IEEE Trans. Ind. Electron.*, vol. 58, no. 1, pp. 95–104, Jan. 2011.

[15] P. C. Loh, D. Li, Y. K. Chai, and F. Blaabjerg, “Autonomous control of interlinking converter with energy storage in hybrid ac–dc Microgrid,” *IEEE Trans. Ind. Appl.*, vol. 49, no. 3, pp. 1374–1382, May/Jun. 2013.

[16] S. Anand, B. G. Fernandes, and J. M. Guerrero, “Distributed control to ensure proportional load sharing and improve voltage regulation in low-voltage dc Microgrids,” *IEEE Trans. Power Electron.*, vol. 28, no. 4, pp. 1900–1913, Apr. 2013.

[17] J. Schönberger, R. Duke, and S. D. Round, “DC-bus signaling: a distributed control strategy for a hybrid renewable Nanogrid,” *IEEE Trans. Ind. Electron.*, vol. 53, no. 5, pp. 1453–1460, Oct. 2006.

[18] D. Chen, L. Xu, L. Yao, “DC voltage variation based autonomous control of dc Microgrids,” *IEEE Trans. Power Del.*, vol. 28, no. 2, pp. 637–648, Apr. 2013.

[19] P. Karlsson and J. Svensson, “DC bus voltage control for a distributed power system,” *IEEE Trans. Power Electron.*, vol. 18, no. 6, pp. 1405–1412, Nov. 2003.

[20] Y. Ito, Y. Zhongqing, and H. Akagi, “DC Microgrid based distribution power generation system,” in *Proc. 4th Int. Power Electron. Motion Control Conf. (IPEMC)*, 2004, pp. 1740–1745.

[21] X. Lu, K. Sun, J. M. Guerrero, J. C. Vasquez, and L. Huang, “State-of-charge balance using adaptive-droop control for distributed energy storage systems in dc Microgrid applications,” *IEEE Trans. Ind. Electron.*, vol. 61, no. 6, pp. 2804–2815, June 2014.

[22] R. A. F. Ferreira, H. A. C. Braga, A. A. Ferreira, and P. G. Barbosa, “Analysis of voltage droop control method for dc Microgrids with Simulink: modeling and simulation,” in *Proc. 10th IEEE/IAS Int. Conf. Ind. Appl. (INDUSCON)*, 2012, pp. 1–6.

[23] J. A. P. Lopes, C. L. Moreira, and A. G. Madureira, “Defining control strategies for Microgrids islanded operation,” *IEEE Trans. Power Syst.*, vol. 21, no. 2, pp. 916–924, May 2006.

[24] A. Tuladhar, H. Jin, T. Unger, and K. Mauch, “Control of parallel inverters in distributed ac power systems with consideration of line impedance effect,” *IEEE Trans. Ind. Appl.*, vol. 36, no. 1, pp. 131–138, Jan./Feb. 2000.

[25] Y. Mohamed and E. F. El-Saadany, “Adaptive decentralized droop controller to preserve power sharing stability of paralleled inverters in distributed generation Microgrids,” *IEEE Trans. Power Electron.*, vol. 23, no. 6, pp. 2806–2816, Nov. 2008.

[26] J. Kim, J. M. Guerrero, P. Rodriguez, R. Teodorescu, and K. Nam, “Mode adaptive droop control with virtual output impedances for an inverter-based flexible ac Microgrid, *IEEE Trans. Power Electron.*, vol. 26, no. 3, pp. 689–701, Mar. 2011.

[27] N. R. Chaudhuri and B. Chaudhuri, “Adaptive droop control for effective power sharing in multi-terminal dc (MTDC) grids,” *IEEE Trans. Power Syst.*, vol. 28, no. 1, pp. 21–29, Feb. 2013.

[28] S. Y. Yang, C. W. Zhang, X. Zhang, R. X. Cao, and W. X. Shen, “Study on the control strategy for parallel operation of inverters based on adaptive droop method,” in *Proc. IEEE Conf. Ind. Electron.ics Appl.*, 2009, pp.1–5.

[29] J. Yuan, F. Gao, H. Gao, H. Zhang, and J. Wu, “An adaptive control strategy for parallel operated photovoltaic inverters,” in *Proc. 7th Int. Power Electron. Motion. Control Conf. (IPEMC)*, 2012, pp. 1522–1526.

[30] R. Majumder, A. Ghosh, G. Ledwich, F. Zare, “Power system stability and load sharing in distributed generation,” in *Proc. IEEE Joint Int. Conf. Power Syst. Technol.*, 2008, pp.1–6.

[31] W. Yao, M. Chen, M. Gao, and Z. Qian, “A wireless load sharing controller to improve the performance of parallel-connected inverters,” in *Proc. IEEE 23rd Annu Applied Power Electron. Conf. Expo. (APEC)*, 2008, pp. 1628–1631.

[32] W. Yao, M. Chen, M. Gao, and Z. Qian, “Development of communicationless hot-swap paralleling for single-phase UPS inverters based on adaptive droop method,” in *Proc. IEEE 23rd Annu Applied Power Electron. Conf. Expo. (APEC*), 2009, pp. 1283–1287.

[33] J. C. Vasquez, J. M. Guerrero, E. Gregorio, P. Rodriguez, R. Teodorescu, F. Blaabjerg, “Adaptive-droop control applied to distributed generation inverters connected to the grid,” in *Proc. IEEE Int. Symp. Ind. Electron. (ISIE), 2008*, pp.2420–2425.

[34] J. C. Vasquez, J. M. Guerrero, A. Luna, P. Rodriguez, and R. Teodorescu, “Adaptive-droop control applied to voltage-source inverters operating in grid-connected and islanded modes,” *IEEE Trans. Ind. Electron.*, vol. 56, no. 10, pp. 4088–4096, Oct. 2009.

[35] A. D. Erdogan and M. T. Aydemir, “Application of adaptive-droop method to boost converters operating at the output of fuel cells,” in *Proc. Int. Elec. Electron. Eng. Conf. (ELECO)*, 2009, pp.I-321–I-325.

[36] T. Dragicevic, J. M. Guerrero, J. C. Vasquez, and D. Skrlec, “Supervisory control of an adaptive-droop regulated dc Microgrid with battery management capability,” *IEEE Trans. Power Electron.*, vol. 29, no. 2, pp. 695–706, Feb. 2014.

[37] H. Liu, Z. Hu, Y. Song, and J. Lin, “Decentralized vehicle-to-grid control for primary frequency regulation considering charging demands,” *IEEE Trans. Power Syst.*, vol. 28, no. 3, pp. 3480–3489, Aug. 2013.

[38] S. Anand and B. G. Fernandes, “Steady state performance analysis for load sharing in dc distributed generation system,” in Proc. *10th Int. Conf. Environment Elect. Eng. (EEEIC)*, 2011, pp. 1–4.

[39] Y. W. Li and C. N. Kao, “An accurate power control strategy for power-electronics-interfaced distributed generation units operation in a low voltage multi-bus Microgrid,” *IEEE Trans. Power Electron.*, vol. 24, no. 12, pp. 2977–2988, Dec. 2009.

[40] J. He and Y. W. Li, “Analysis, design and implementation of virtual impedance for power electronics interfaced distributed generation,” *IEEE Trans. Ind. Appl.*, vol. 47, no. 6, pp. 2525–2538, Nov./Dec. 2011.

[41] W. Qiu and Z. Liang, “Practical design considerations of current sharing control for parallel VRM applications,” in *Proc. 20th Annu. Appl. Power Electron. Conf. Expo.*, 2005, pp. 281–286.

[42] H. Laaksonen, P. Saari, and R. Komulainen, “Voltage and frequency control of inverter based weak LV network Microgrid,” in *Proc. Int. Conf. Future Power Syst.*, 2005, pp. 1–6.

[43] T. L. Vandoorn, B. Meersman, L. Degroote, B. Renders, and L. Vandevelde, “A control strategy for islanded Microgrids with dc-link voltage control,” *IEEE Trans. Power Del.*, vol. 26, no. 2, pp. 703–713, Apr. 2011.

[44] Q. Shafiee, J. M. Guerrero, and J. C. Vasquez, “Distributed secondary control for islanded Microgrids – A novel approach,” *IEEE Trans. Power Electron.*, vol. 29, no. 2, pp. 1018–1031, Feb. 2014.

[45] X. Lu, J. M. Guerrero, K. Sun, and J. C. Vasquez, “An improved droop control method for dc Microgrids based on low bandwidth communication with dc bus voltage restoration and enhanced current sharing accuracy,” *IEEE Trans. Power Electron.*, vol. 29, no. 4, pp. 1800–1812, Apr. 2014.

[46] V. Nasirian, S. Moayedi, A. Davoudi, and F. L. Lewis, “Distributed cooperative control of dc Microgrids,” *IEEE Trans. Power Electron.*, to be published, DOI: 10.1109/TPEL.2014.2324579.

[47] R. Olfati-Saber and R. M. Murray, "Consensus problems in networks of agents with switching topology and time-delays," *IEEE Trans. Autom. Control*, vol. 49, no. 9, pp. 1520–1533, Sept. 2004.

[48] D. P. Spanos, R. Olfati-Saber, and R. M. Murray, "Dynamic consensus for mobile networks," in *Proc. 16th Int. Fed. Aut. Control (IFAC)*, 2005, pp. 1–6.

[49] R. W. Erickson and D. Maksimovic, *Fundamental of Power Electronics*, 2nd Ed. Norwell, MA: Kluwer, 2001.

[50] V. Nasirian, Y. Karimi, A. Davoudi, M. R. Zolghadri, M. Ahmadian, and S. Moayedi, "Dynamic model development and variable switching-frequency control for DCVM Cúk converters in PFC applications," *IEEE Trans. Ind. Appl.*, vol. 49, no. 6, pp. 2636–2650, Nov./Dec. 2013.

[51] S. Moayedi, V. Nasirian, F. L. Lewis, and A. Davoudi, "Team-oriented load sharing in parallel dc-dc converters" *IEEE Trans. Ind. Electron.*, to be published, DOI: 10.1109/TIA.2014.2336982.

[52] J. M. Guerrero, M. Chandorkar, T. Lee, and P. C. Loh, "Advanced control architectures for intelligent Microgrids—part I: decentralized and hierarchical control," *IEEE Trans. Ind. Electron.*, vol. 60, no. 4, pp. 1254–1262, Apr. 2013.

[53] D. Nilsson and A. Sannino, "Efficiency analysis of low- and medium voltage dc distribution systems," in *Proc. IEEE Power Eng. Soc. Gen. Meeting*, 2004, pp. 2315–2321.

[54] S. Anand and B. G. Fernandes, "Optimal voltage level for dc Microgrids," in *Proc. 36th Annu. Conf. IEEE Ind. Electron. Soc. (IECON)*, 2010, pp. 3034–3039.

[55] N. Amelina and A. Fradkov, "Consensus problem in stochastic network systems with switched topology, noise, and delay," in *Proc. 12th Int. Conf. Network*, 2013, pp. 118–124.

[56] R. Olfati-Saber and R. M. Murray, "Consensus problems in networks of agents with switching topology and time-delays," *IEEE Trans. Automat. Control*, vol. 49, no. 9, pp. 1520–1533, Sept. 2004.

[57] S. Kar and J. M. F. Moura, "Distributed consensus algorithms in sensor networks with imperfect communication: link failures and channel noise," *IEEE Trans. Signal Process.*, vol. 57, no. 1, pp. 355–369, Jan. 2009.

Vahidreza Nasirian (S'12) received the B.S. and M.S. degrees in electrical engineering from Sharif University of Technology, Tehran, Iran, in 2007 and 2010, respectively. He is currently working toward the Ph.D. degree at The University of Texas at Arlington, Arlington, TX, USA.

His research interests include the modeling and control of power electronics and electric drives, microgrid control, transportation electrification, and renewable and sustainable energy systems.

Mr. Nasirian was the recipient of the gold medal at the 20th National Mathematics Olympiad in 2002 in Tehran, Iran, and the bronze medal at the 2nd Silk Road Mathematics Competition in 2003 in Turkey. He was also the recipient of the Iranian National Elites Foundation Fellowship for 2008–2010 and the Carrizo Oil & Gas Inc. Graduate Research Fellowship for 2011–2013.

Ali Davoudi (S'04–M'11) is currently an Assistant Professor at the Electrical Engineering department of the University of Texas-Arlington. He received his Ph.D. in Electrical and Computer Engineering from the University of Illinois, Urbana-Champaign, USA, in 2010. He worked for Solar Bridge Technologies, Texas Instruments Inc., and Royal Philips Electronics.

He is an Associate Editor for IEEE TRANSACTIONS ON INDUSTRY APPLICATIONS and IEEE TRANSACTIONS ON TRANSPORTATION ELECTRIFICATION. He was a guest editor for IEEE TRANSACTIONS ON SMARTGRID, special issue on Smart DC distribution Systems; IEEE TRANSACTIONS ON VEHICULAR TECHNOLOGY, special issue on Advanced modeling, simulation, control and optimization paradigms for vehicular power systems; and IEEE TRANSACTIONS ON ENERGY CONVERSION, special issue on Advanced distributed control of energy conversion devices and systems. His research interests are various aspects of modeling and control of power electronics and finite-inertia power systems.

Frank L. Lewis (F'94) is currently with The University of Texas at Arlington (UTA), Arlington, TX, USA. He works in feedback control, reinforcement learning, intelligent systems, and distributed control systems. He is the author of 273 journal papers, 375 conference papers, 15 books, 44 chapters, and 11 journal special issues and is the holder of 6 U.S. patents.

Dr. Lewis is a member of the National Academy of Inventors, a Fellow of IFAC and the U.K. Institute of Measurement and Control, a Professional Engineer in the State of Texas, and a U.K. Chartered Engineer. He is also a UTA Distinguished Scholar Professor, a UTA Distinguished Teaching Professor, and the Moncrief-O'Donnell Chair at The University of Texas at Arlington Research Institute. He is also an IEEE Control Systems Society Distinguished Lecturer. He received the Fulbright Research Award, NSF Research Initiation Grant, ASEE Terman Award, International Neural Network Society Gabor Award in 2009, and U.K. Institute of Measurement and Control Honeywell Field Engineering Medal in 2009. He received the IEEE Computational Intelligence Society Neural Networks Pioneer Award in 2012. He was a Distinguished Foreign Scholar of the Nanjing University of Science and Technology. He was also a Project 111 Professor at Northeastern University, China. He received the Outstanding Service Award from the Dallas IEEE section and was selected as Engineer of the Year by the Fort Worth IEEE Section. He was listed in the Fort Worth Business Press Top 200 Leaders in Manufacturing. He received the 2010 IEEE Region 5 Outstanding Engineering Educator Award and the 2010 UTA Graduate Dean's Excellence in Doctoral Mentoring Award. He was elected to the UTA Academy of Distinguished Teachers in 2012. He served on the NAE Committee on Space Station in 1995. He is the Founding Member of the Board of Governors of the Mediterranean Control Association. He helped win the IEEE Control Systems Society Best Chapter Award (as Founding Chairman of the DFW Chapter), the National Sigma Xi Award for Outstanding Chapter (as President of the UTA Chapter), and the U.S. SBA Tibbetts Award in 1996 (as Director of ARRI's SBIR Program).

Josep M. Guerrero (S'01-M'04-SM'08) received the B.S. degree in telecommunications engineering, the M.S. degree in electronics engineering, and the Ph.D. degree in power electronics from the Technical University of Catalonia, Barcelona, in 1997, 2000 and 2003, respectively. Since 2011, he has been a Full Professor with the Department of Energy Technology, Aalborg University, Denmark, where he is responsible for the Microgrid Research Program. From 2012 he is a guest Professor at the Chinese Academy of Science and the Nanjing University of Aeronautics and Astronautics; and from 2014 he is chair Professor in Shandong University.

His research interest is oriented to different microgrid aspects, including power electronics, distributed energy-storage systems, hierarchical and cooperative control, energy management systems, and optimization of microgrids and islanded minigrids.

Prof. Guerrero is an Associate Editor for the IEEE TRANSACTIONS ON POWER ELECTRONICS, the IEEE TRANSACTIONS ON INDUSTRIAL ELECTRONICS, and the IEEE Industrial Electronics Magazine, and an Editor for the IEEE TRANSACTIONS ON SMARTGRID. He has been a Guest Editor for the IEEE TRANSACTIONS ON POWER ELECTRONICS Special Issues: Power Electronics for Wind Energy Conversion and Power Electronics for Microgrids; the IEEE TRANSACTIONS ON INDUSTRIAL ELECTRONICS Special Sections: Uninterruptible Power Supplies systems, Renewable Energy Systems, Distributed Generation and Microgrids, and Industrial Applications and Implementation Issues of the Kalman Filter; and the IEEE TRANSACTIONS ON SMARTGRID Special Issue on Smart DC Distribution Systems. He was the chair of the Renewable Energy Systems Technical Committee of the IEEE Industrial Electronics Society. In 2014 he was awarded as ISI Highly Cited Researcher.